Laser & Photonics Reviews

LASER & PHOTONICS REVIEWS

www.lpr-journal.org

RESEARCH ARTICLE OPEN ACCESS

The Polarizability Vector: A Polarimetric Observable for Characterizing Anisotropic Nanoparticles

Jorge Olmos-Trigo[1,2]

[1]Departamento de Física de Materiales, Universidad Autonoma de Madrid (UAM), Madrid 28049, Spain | [2]Faculty of Optics and Optometry, Universidad Complutense de Madrid, Madrid 28037, Spain

Correspondence: Jorge Olmos-Trigo (jorge.olmos@uam.es)

Received: 26 June 2025 | **Revised:** 28 September 2025 | **Accepted:** 10 October 2025

Keywords: nanoparticles | nanophotonics | plasmonics | polarimetry | stokes vector

ABSTRACT

The optical properties of anisotropic nanoparticles (NPs) are often characterized by two principal components of their polarizability tensor. However, measuring them can be demanding as the phase of the scattered field needs to be detected. To address this challenge, I reveal a novel observable, the polarizability vector $\boldsymbol{\mathcal{P}}$, for characterizing the optical response of anisotropic NPs from a single-angle Stokes vector measurement. As I show, knowledge of $\boldsymbol{\mathcal{P}}$ grants access to pivotal nanophotonics quantities, including the scattering cross-section, optical recoil torque, and near-field amplitude. I further generalize the approach to randomly dispersed NPs, showing that $\boldsymbol{\mathcal{P}}$, though defined at the single-particle level, fully captures their optical response. My findings pave the way for the optical characterization of anisotropic NPs using standard polarimetric instrumentation.

1 | Introduction

The polarizability tensor $\overline{\alpha}$ of nanoparticles (NPs) governs their interaction with electromagnetic fields. For example, the plasmon resonance of metallic NPs, the hallmark of their optical response [1–7], is fully encoded in $\overline{\alpha}$. NPs described by point-electric dipoles exhibit a 3×3 tensor. However, when these are made of homogeneous and isotropic materials, $\overline{\alpha}$ can be diagonalized in the coordinate frame defined by their principal axes [8], taking the form of:

$$\overline{\alpha} = \begin{pmatrix} \alpha_1 & 0 & 0 \\ 0 & \alpha_2 & 0 \\ 0 & 0 & \alpha_3 \end{pmatrix}$$

Here, α_1, α_2, and α_3 are the principal components of $\overline{\alpha}$, namely, complex-valued numbers which only depend on the geometry and the material of the anisotropic NP.

A common experimental configuration involves depositing the NPs on a substrate and tailoring the incident illumination to selectively excite just two components of $\overline{\alpha}$, for instance, α_1 and α_2 [9, 10]. These polarizabilities are calculated using exact numerical tools such as the T-matrix method [11, 12], the surface integral method [13], Maxwell solvers [14], or Mie's theory in the case of spherical NPs [15–17]. However, the experimental determination of α_1 and α_2 can be challenging [18–22], as it requires detecting not only the amplitude but also the phase of the scattered field through quantitative phase measurements [23–30]. Researchers typically rely on more accessible approaches for characterizing some of the optical properties of NPs. These are usually based on measuring the extinction, scattering, and/or absorption cross-sections [31–37]. However, these cross-sections provide partial information about α_1 and α_2, hindering crucial information about the optical response of NPs.

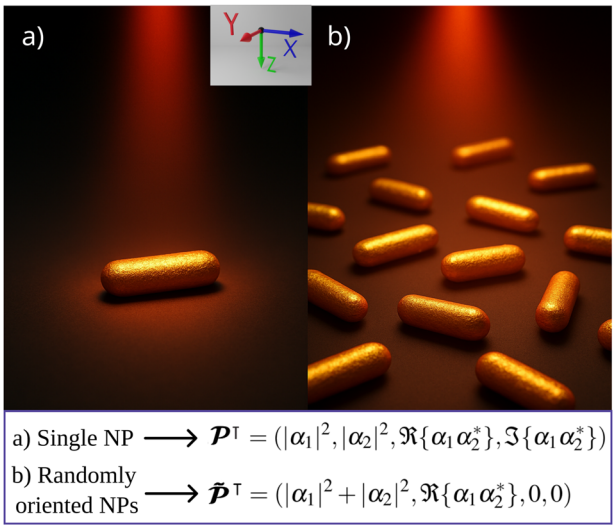

FIGURE 1 | Sketch of the light-scattering systems considered in this work. a) A single NP. b) Randomly oriented NPs. I also show the polarizability vectors attainable for each configuration.

These drawbacks highlight the need for an observable to characterize the optical response of anisotropic NPs. In this work, I find an overlooked observable in nanophotonics, hereafter referred to as the *polarizability vector* $\boldsymbol{\mathcal{P}}$, given by:

$$\boldsymbol{\mathcal{P}}^\intercal = (|\alpha_1|^2, |\alpha_2|^2, \Re\{\alpha_1\alpha_2^*\}, \Im\{\alpha_1\alpha_2^*\}) \tag{1}$$

Here $\Re$ and $\Im$ are the real and imaginary parts, respectively.

Notably, I demonstrate that $\boldsymbol{\mathcal{P}}$ can be retrieved from a single-angle Stokes vector measurement. This technique can accommodate general illumination conditions, applies to NPs made of any homogeneous material and in any orientation, and can be validated in situ by measuring the Stokes vector at two distinct non-forward angles of choice. As I show, knowledge of $\boldsymbol{\mathcal{P}}$ enables access to a broad class of relevant quantities in nanophotonics that depend quadratically on $\overline{\alpha}$, such as the scattering cross-section, optical recoil torque, and near-field amplitude.

Finally, I extend this framework to random dispersions of non-interacting NPs. Specifically, I find that a measurement of the rotationally averaged Stokes vector at a single collection angle provides key information of these dispersions, such as their scattering cross-section and optical recoil torque. In addition to this, I show that $\boldsymbol{\mathcal{P}}$, defined at the single-particle level, fully captures the optical response of such dispersions. However, the converse does not hold: averaging obscures information about the components of $\boldsymbol{\mathcal{P}}$ given in Equation (1).

Next, I introduce the framework used in this work.

2 | The Polarizability Tensor in the Laboratory Frame

I consider an anisotropic NP lying flat on a substrate excited by a propagating beam in the z-direction, as shown in Figure 1a. Following the standard practice for a subwavelength NP, I model its optical response as an electric-point dipole $\mathbf{p}$:

$$\mathbf{p} = \epsilon_h \epsilon_0 \overline{\alpha}_{\text{lab}} \mathbf{E}_{\text{i}} \tag{2}$$

Here, ϵ_h is the dimensionless permittivity of the surrounding medium, ϵ_0 is the vacuum permittivity, and $\mathbf{E}_{\text{i}} = E_x\hat{\mathbf{e}}_x + E_y\hat{\mathbf{e}}_y$ is the incident electromagnetic field, where E_x and E_y are the complex-valued amplitudes of the Jones vector [8]. In the laboratory frame of reference, fixed relative to the incident beam $\mathbf{E}_{\text{i}}$, the polarizability tensor $\overline{\alpha}_{\text{lab}}$ of the NP can be derived from $\overline{\alpha}$ and takes the form of [38]:

$$\overline{\alpha}_{\text{lab}} = \overline{R}_z(\beta)\,\overline{\alpha}\,\overline{R}_z^{\intercal}(\beta) = \begin{pmatrix} \alpha_{xx} & \alpha_{xy} & 0 \\ \alpha_{yx} & \alpha_{yy} & 0 \\ 0 & 0 & \alpha_{zz} \end{pmatrix} \tag{3}$$

where $\overline{R}_z(\beta)$ is the rotation matrix over the z-axis [38]. The polarizability tensor given in Equation (3) embodies a reciprocal ($\overline{\alpha}_{\text{lab}} = \overline{\alpha}_{\text{lab}}^{\intercal}$) but anisotropic optical response and its components are $\alpha_{xx} = \alpha_1\cos^2\beta + \alpha_2\sin^2\beta$, $\alpha_{yy} = \alpha_2\cos^2\beta + \alpha_1\sin^2\beta$, $\alpha_{zz} = \alpha_3$, and $\alpha_{xy} = \alpha_{yx} = (\alpha_1 - \alpha_2)\sin\beta\cos\beta$. Note that for $\beta = m\pi$ and $\beta = m\pi/2$, where $m \in \mathbb{Z}$, the principal axes of the NP are aligned with $\mathbf{E}_{\text{i}}$, yielding a diagonal tensor, namely, $\alpha_{xy} = \alpha_{yx} = 0$.

In the following, I determine $\boldsymbol{\mathcal{P}}$ introduced in Equation (1) using the Stokes vector $\mathbf{S}$ produced by the NP. Since $\mathbf{S}$ depends on the scattered field by the NP, I first introduce this field.

3 | The Electromagnetic Radiation Produced by the NP

The scattered field produced by a electric-point dipole $\mathbf{p}$ in the radiation (far) zone reads as [39, Equation 9.19]:

$$\mathbf{E}_{\text{sca}} = \frac{k^2 e^{ikr}}{4\pi r}\left(\hat{\mathbf{e}}_r \times \frac{\mathbf{p}}{\epsilon_h\epsilon_0}\right) \times \hat{\mathbf{e}}_r \tag{4}$$

Here, $k = (2\pi/\lambda_0)n_h$, where $n_h = \sqrt{\epsilon_h}$, λ_0 is the incident wavelength, $\hat{\mathbf{e}}_r$ is the radial unit vector, and r is the distance from the center of the NP. The scattered field given in Equation (4) can be calculated from the electric-point dipole $\mathbf{p}$ given in Equation (2). However, $\mathbf{p}$ is not an observable, rendering $\mathbf{E}_{\text{sca}}$ often undetectable in practice.

To gain insights into the optical response of the NP, I now turn to experimentally accessible observables. As previously announced, I consider the Stokes vector $\mathbf{S}$, which describes the polarization state of the scattered field given in Equation (4). The components of the Stokes vector $\mathbf{S}^\intercal = [s_0, s_1, s_2, s_3]$, known as the Stokes parameters, depend only on the transverse components of the scattered field, i.e., $E_\theta = \mathbf{E}_{\text{sca}} \cdot \hat{\mathbf{e}}_\theta$ and $E_\varphi = \mathbf{E}_{\text{sca}} \cdot \hat{\mathbf{e}}_\varphi$ [40–44]. Here θ and φ denote the scattering and azimuth angles, respectively, and the "$^\intercal$" symbol denotes the "transpose" operation. Moreover, $\hat{\mathbf{e}}_\theta$ and $\hat{\mathbf{e}}_\varphi$ denote the scattering and azimuth unit vectors, respectively. Note that I use the same convention as Jackson's

book [39]. In this framework, $\mathbf{S}$ is expressed in terms of E_θ and E_φ as [45]:

$$s_0 = |E_\theta|^2 + |E_\varphi|^2, \qquad s_1 = |E_\theta|^2 - |E_\varphi|^2$$
$$s_2 = -2\Re\{E_\theta E_\varphi^*\}, \qquad s_3 = 2\Im\{E_\theta E_\varphi^*\}$$

Here, s_0 denotes the total scattered intensity, s_1 is the degree of linear polarization, s_2 is the degree of linear polarization at 45° degrees, and s_3 denotes the degree of circular polarization.

Next, I discuss how the Stokes vector $\mathbf{S}$ can be used to determine the polarizability vector $\boldsymbol{\mathcal{P}}$ given in Equation (1).

4 | Simple, Versatile, and Robust Polarimetry of a Geometrically Anisotropic NP

It is well-known that the polarizabilities α_1 and α_2 only depend on intrinsic properties of the NP, such as material and shape [8]. However, the Stokes vector $\mathbf{S}$ also depends on external parameters, such as the collection angles (θ, φ) and the dimensionless optical distance kr. To attain $\boldsymbol{\mathcal{P}}$, I now perform a two-step transformation that progressively removes the dependence on these external parameters.

The first step consists of finding a matrix transformation $\overline{\mathbf{U}}_1(\theta, \varphi, kr)$ that relates the Stokes vector $\mathbf{S}$ with a new dipolar vector $\mathbf{D}^\intercal = \left(|p_x|^2, |p_y|^2, \Re\{p_x p_y^*\}, \Im\{p_x p_y^*\}\right)$. The latter vector is independent of the collection angles and the optical distance. This transformation can be expressed as:

$$\mathbf{D}(\alpha_1, \alpha_2, \mathbf{E}_\mathrm{i}, \beta) = \overline{\mathbf{U}}_1(\theta, \varphi, kr)\, \mathbf{S}(\alpha_1, \alpha_2, \mathbf{E}_\mathrm{i}, \beta, \theta, \varphi, kr) \tag{5}$$

The second step eliminates the dependence on $\mathbf{E}_\mathrm{i}$ and β. This can be achieved by applying a second matrix transformation $\overline{\mathbf{U}}_2(\mathbf{E}_\mathrm{i}, \beta)$ that connects $\mathbf{D}$ with $\boldsymbol{\mathcal{P}}$:

$$\boldsymbol{\mathcal{P}}(\alpha_1, \alpha_2) = \overline{\mathbf{U}}_2(\mathbf{E}_\mathrm{i}, \beta)\, \mathbf{D}(\alpha_1, \alpha_2, \mathbf{E}_\mathrm{i}, \beta) \tag{6}$$

Combining Equations (5) and (6), I obtain the full transformation from $\mathbf{S}$ to $\boldsymbol{\mathcal{P}}$, namely,

$$\boldsymbol{\mathcal{P}}(\alpha_1, \alpha_2) = \overline{\mathbf{U}}_2(\mathbf{E}_\mathrm{i}, \beta)\, \overline{\mathbf{U}}_1(\theta, \varphi, kr)\, \mathbf{S}(\alpha_1, \alpha_2, \mathbf{E}_\mathrm{i}, \beta, \theta, \varphi, kr) \tag{7}$$

Equation (7) embodies the polarimetry method presented in this work. It relates a measurement of the Stokes vector $\mathbf{S}(\alpha_1, \alpha_2, \mathbf{E}_\mathrm{i}, \beta, \theta, \varphi, kr)$ at a single collection angle with the polarizability vector $\boldsymbol{\mathcal{P}}(\alpha_1, \alpha_2)$. As Equation (7) evidences, the problem reduces to finding the transformation matrices $\overline{\mathbf{U}}_1(\theta, \varphi, kr)$ and $\overline{\mathbf{U}}_2(\mathbf{E}_\mathrm{i}, \beta)$. The derivation of such matrices can be found in Appendix A and Appendix B, respectively.

I now highlight the most important features of Equation (7). To start with, it can be used under a wide variety of illuminations since no requirements have been imposed on the Jones vector defined by $\mathbf{E}_\mathrm{i}$. Moreover, the NP can be arbitrarily oriented, meaning that no alignment mechanism is needed to control the orientational angle β [46–51]. Furthermore, the NP and surrounding medium can be made of any non-active homogeneous material [52]. Note that the only requirement I impose is that the optical response of the NP can be described by the electric-point dipole $\mathbf{p}$ given in Equation (2).

A key strength of my polarimetry-based method given in Equation (7) is its robustness. Specifically, the technique can be experimentally verified in situ by using Equation (7) at two different collection angles. If the retrieved $\boldsymbol{\mathcal{P}}(\alpha_1, \alpha_2)$ remains identical after these two Stokes measurements, then the electromagnetic properties of the NP are accurately characterized.

Next, I provide an illustrative example to demonstrate the reach of the method. In particular, I determine $\boldsymbol{\mathcal{P}}(\alpha_1, \alpha_2)$ produced by one of the most versatile light-scattering systems in Nanophotonics: a gold nanorod excited by an arbitrarily polarized plane-wave with $\mathbf{E}_\mathrm{i} = (E_x, E_y, 0)e^{ikz}$ [53–62].

Figure 2 shows the calculated components of $\boldsymbol{\mathcal{P}}(\alpha_1, \alpha_2)$, as given in Equation (1), normalized by the volume squared V^2 of the nanorod, as a function of the incident wavelength λ_0. The nanorod has a short semi-axis $a = 25$ nm and a long semi-axis $c = 30$ nm, and it is surrounded by water ($n_h = 1.33$). Each panel corresponds to a different component of $\boldsymbol{\mathcal{P}}(\alpha_1, \alpha_2)$: (a) $|\alpha_1|^2$, (b) $|\alpha_2|^2$, (c) $\Re\{\alpha_1\alpha_2^*\}$, and (d) $\Im\{\alpha_1\alpha_2^*\}$. Colored dashed and dotted curves represent the four simulated cases, calculated using Equation (7), with parameters provided in Table 1. The solid black line corresponds to the numerical calculation using the exact T-matrix method [63, 64]. As Figure 2 shows, the agreement between the exact solution and all simulated cases of Table 1 is remarkable. Note that cases 1 and 2, as well as cases 3 and 4, share the same incident field $\mathbf{E}_\mathrm{i}$ and nanorod's orientation β, differing only in the collection angles. The fact that all cases given in Table 1 lead to the same $\boldsymbol{\mathcal{P}}(\alpha_1, \alpha_2)$ serves as an explicit demonstration of the robustness of the method. For completeness, I show in Figure 3 the same quantities as in Figure 2, but for a silver prolate spheroid with a = 20 nm and c = 25 nm.

Next, I discuss how much information can be extracted from $\boldsymbol{\mathcal{P}}(\alpha_1, \alpha_2)$. From now on, the variable dependencies in all quantities will be assumed and omitted from the notation.

5 | How much Information can be Extracted from $\boldsymbol{\mathcal{P}}$?

The first key observation is that $\boldsymbol{\mathcal{P}}$ reveals the asymmetries of the NP. Specifically, one can note that the NP is spherical if and only if $\mathcal{P}_0 = \mathcal{P}_1 = \mathcal{P}_2$ and $\mathcal{P}_3 = 0$. Such a bi-univocal relation can be used to probe the sphericity of NPs using polarimetry alone. Note that $\mathcal{P}_i$ is the i-component of the $\boldsymbol{\mathcal{P}}$, e.g., $\mathcal{P}_1 = |\alpha_2|^2$. Moreover, for non-spherical NPs, one can distinguish between their long and short principal axes by comparing the first two components of $\boldsymbol{\mathcal{P}}$. That is, one can check whether $|\alpha_1| > |\alpha_2|$ or $|\alpha_1| < |\alpha_2|$ using $\mathcal{P}_0$ and $\mathcal{P}_1$.

Next, I will use $\boldsymbol{\mathcal{P}}$ to capture a broad class of physically relevant quantities that are often difficult to measure.

I start with a central quantity in Physics: the scattering cross-section σ_sca, which, among other features, captures the optical resonances of NPs. In general, σ_sca is computed by averaging

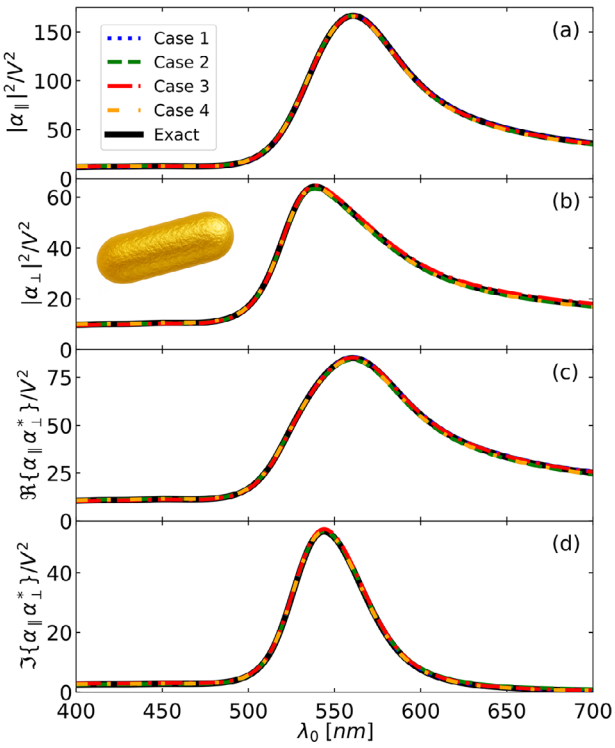

FIGURE 2 | Calculated components of the polarizability vector $\boldsymbol{\mathcal{P}}$ given in Equation (1), normalized by the volume squared $V^2 = ((4\pi/3)a^2c)^2$ of the gold nanorod, as a function of the incident wavelength λ_0. The nanorod has a short semi-axis of a = 25 nm and a long semi-axis of c = 30 nm. Each panel corresponds to a different component: (a) $|\alpha_1|^2$, (b) $|\alpha_2|^2$, (c) $\Re\{\alpha_1\alpha_2^*\}$, and (d) $\Im\{\alpha_1\alpha_2^*\}$. Colored dashed and dotted curves correspond to the four simulated cases employing Equation (7), whose parameters are detailed in Table 1. The solid black line represents the exact calculation using the T-matrix method. Case numbers are color-coded consistently with the legend and Table 1.

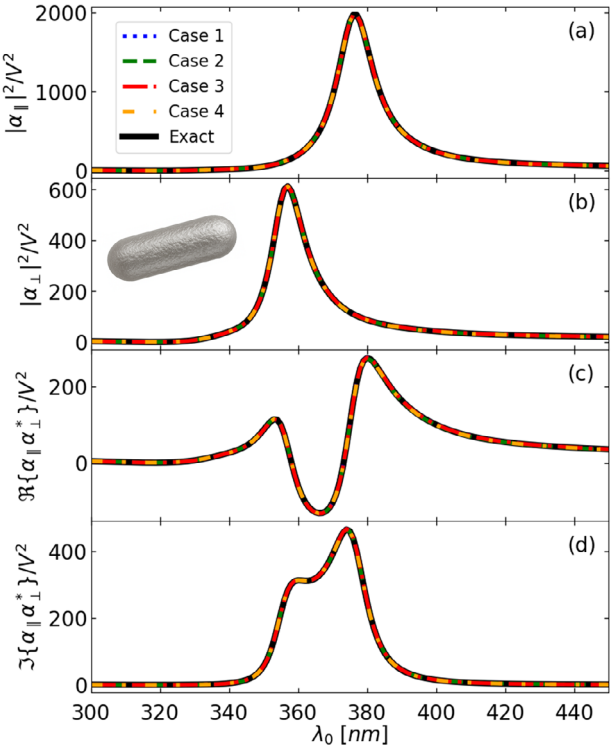

FIGURE 3 | Calculated components of the polarizability vector $\boldsymbol{\mathcal{P}}$ given in Equation (1), normalized by the volume squared $V^2 = ((4\pi/3)a^2c)^2$ of the silver nanorod, as a function of the incident wavelength λ_0. The nanorod has a short semi-axis of a = 20 nm and a long semi-axis of c = 25 nm. Each panel corresponds to a different component: (a) $|\alpha_1|^2$, (b) $|\alpha_2|^2$, (c) $\Re\{\alpha_1\alpha_2^*\}$, and (d) $\Im\{\alpha_1\alpha_2^*\}$. Colored dashed and dotted curves correspond to the four simulated cases employing Equation (7), whose parameters are detailed in Table 1. The solid black line represents the exact calculation using the T-matrix method. Case numbers are color-coded consistently with the legend and Table 1.

the amplitude of the scattered field in all directions using an integrating sphere embedding the NP in far-field [8]. For dipolar NPs, this calculation yields:

$$\sigma_{\text{sca}} = \frac{1}{|\mathbf{E}_{\text{i}}|^2}\int_\Omega |\mathbf{E}_{\text{sca}}|^2 r^2 d\Omega = \frac{k^4}{6\pi|\mathbf{E}_{\text{i}}|^2}\left|\frac{\mathbf{p}}{\epsilon_h\epsilon_0}\right|^2 \tag{8}$$

Inspecting Equation (8), one can notice that σ_{sca} can be determined from $\boldsymbol{\mathcal{P}}$ for any combination of $(\mathbf{E}_{\text{i}}, \beta)$. That is, once $\boldsymbol{\mathcal{P}}$ has been retrieved for a specific $(\mathbf{E}_{\text{i}}, \beta)$, it can be used to determine σ_{sca} for other illuminations $\mathbf{E}'_{\text{i}}$ and orientations β' of the NP.

TABLE 1 | Parameters for each calculated case in Figures 2 and 3: angles θ, ϕ, and β (all in deg) and incident field components E_x and E_y. The numbers are color-coded according to the plot legend in Figures 2 and 3.

Case	θ (deg)	ϕ (deg)	β (deg)	E_x (E_0)	E_y (E_0)
1	160	230	60	$1/\sqrt{2}$	$\mathrm{i}/\sqrt{2}$
2	60	30	60	$1/\sqrt{2}$	$\mathrm{i}/\sqrt{2}$
3	150	260	30	0	1
4	50	60	30	0	1

This is because $\boldsymbol{\mathcal{P}}$ only depends on polarizabilities, and these are intrinsic properties of the NP. Notably, this reasoning extends to any quantity derivable from $\boldsymbol{\mathcal{P}}$, not just to σ_{sca}.

In the following, I show two examples of σ_{sca} corresponding to the incident polarizations considered in Table 1. The general case is presented in Appendix C. Now, by expanding Equation (8) using Equations (2) and (3) for $\mathbf{E} = E_0(1, \mathrm{i})/\sqrt{2}$, which corresponds to the circular polarized (CP) light used in cases 1 and 2 of Table 1, one arrives at

$$\sigma_{\text{sca}}^{\text{CP}} = \frac{k^4}{12\pi}\left(|\alpha_1|^2 + |\alpha_2|^2\right) = \frac{k^4}{12\pi}(\mathcal{P}_0 + \mathcal{P}_1)$$

Moreover, by expanding Equation (8) using Equations (2) and (3) for $E_x = 0$ and $E_y = E_0$, which corresponds to the linearly polarized (LP) light employed in cases 3 and 4 of Table 1, one arrives at

$$\sigma_{\text{sca}}^{\text{LP}} = \frac{k^4}{6\pi}\left(\mathcal{P}_0 \sin^2\beta + \mathcal{P}_1 \cos^2\beta\right)$$

As anticipated, σ_{sca} can be obtained from $\boldsymbol{\mathcal{P}}$, which, in turn, can be determined via my polarimetry-based method given in Equation (7). Importantly, this method enables the separation of

$|\alpha_1|^2$ and $|\alpha_2|^2$ in σ_{sca}, something that is not generally possible when σ_{sca} is measured using an integrating sphere [65].

Next, I demonstrate that the polarizability vector $\boldsymbol{\mathcal{P}}$ can be used to capture another quantity without actually measuring it: the recoil optical torque, hereafter denoted as $\boldsymbol{\Gamma}_{rec}$ [66–68]. In general terms, $\boldsymbol{\Gamma}_{rec}$ is calculated by integrating the Maxwell Stress tensor in the far-field [69, 70]. In the dipolar regime and for $p_z = 0$, such a calculation yields [68]

$$\boldsymbol{\Gamma}_{rec} = \frac{k^3}{12\pi\epsilon_h\epsilon_0}\Im\{\mathbf{p}\times\mathbf{p}^*\} = \frac{k^3}{6\pi\epsilon_h\epsilon_0}\Im\{p_x p_y^*\}\hat{\mathbf{e}}_z = \Gamma_{rec}\hat{\mathbf{e}}_z \tag{9}$$

Inspecting Equation (9), one can notice that Γ_{rec} can be captured using $\boldsymbol{\mathcal{P}}$ for any given combination of $(\mathbf{E}_i, \beta)$. While the generic case is derived in Appendix D, I now show the examples corresponding to the cases considered in Table (1).

Expanding Equation (9) using Equations (2) and (3) for $\mathbf{E} = E_0(1, i)/\sqrt{2}$, I have

$$\frac{\Gamma_{rec}^{CP}}{\Gamma_0} = \frac{\Re\{\alpha_1\alpha_2^*\}}{V^2} = \frac{\mathcal{P}_2}{V^2}$$

Here, I have defined $\Gamma_0 = (k^3|E_0|^2\epsilon_h\epsilon_0 V^2)/12\pi$. Moreover, by setting $\mathbf{E}_i = E_0(0, 1)$, I arrive at

$$\frac{\Gamma_{rec}^{LP}}{\Gamma_0} = \frac{\Im\{\alpha_1\alpha_2^*\}\sin 2\beta}{V^2} = \frac{\mathcal{P}_3\sin 2\beta}{V^2}$$

As previously anticipated, one can can determine Γ_{rec} using $\boldsymbol{\mathcal{P}}$ given in Equation (7). These results can facilitate the experimental distinction between the recoil and extinction components of the total optical torque for dipolar NPs [71–74].

Next, I show that $\boldsymbol{\mathcal{P}}$ can also be used to reconstruct the scattered electromagnetic field at all points of the radiation zone. That is, from the far-to-near field. To illustrate this counter-intuitive relation, as $\boldsymbol{\mathcal{P}}$ is calculated from a measurement of $\mathbf{S}$ in the far-field, I now write the scattered field produced by an electric-point dipole $\mathbf{p}$ at any point of the radiation zone excluding the far-field region [39, Equation 9.18]:

$$\mathbf{E}_{sca}^{NF-MD} = \frac{k^2 e^{ikr}}{4\pi r}\frac{[3\hat{\mathbf{e}}_r(\hat{\mathbf{e}}_r\cdot\mathbf{p}) - \mathbf{p}]}{\epsilon_h\epsilon_0}\left(\frac{1-ikr}{(kr)^2}\right)$$

Taking the modulus of the previous equation, I arrive at

$$|\mathbf{E}_{sca}^{NF-MD}|^2 = \frac{1+(kr)^2}{16\pi^2 r^6}\frac{\left(4|p_r|^2 + |p_\theta|^2 + |p_\varphi|^2\right)}{(\epsilon_h\epsilon_0)^2} \tag{10}$$

By using the cartesian-to-spherical transformation (with $p_z = 0$) [39], one can easily express Equation (10) in terms of $\mathbf{D}$. Then, one can link $\mathbf{D}$ with $\boldsymbol{\mathcal{P}}$ using Equation (6). This implies that a single measurement of the Stokes vector $\mathbf{S}$ in the far-field can be used to reconstruct the amplitude of the scattered field produced by an electric-point dipole $\mathbf{p}$ at any point of the radiation zone. This explicit calculation can be found in Appendix E.

Finally, I extend my technique to address one of the most studied systems in nanophotonics: random dispersion of identical and non-interacting NPs.

6 | A Random Dispersion of Identical, Non-Interacting NPs

For a random dispersion of NPs, one needs to calculate the rotationally-averaged Stokes vector produced by them: $N\langle\mathbf{S}\rangle$. Here, N is the number of the excited NPs, and $\langle\mathbf{S}\rangle$ denotes the rotationally-averaged Stokes vector produced by a single NP:

$$\langle\mathbf{S}\rangle = \frac{1}{2\pi}\int_0^{2\pi}\mathbf{S}(\alpha_1, \alpha_2, \mathbf{E}_i, \beta, \theta, \varphi, kr)\, d\beta \tag{11}$$

Some comments are in order. First, one can note that the averaging of Equation (11) does not play a role in the observational angles $\{\theta, \varphi\}$ and the optical distance kr. Therefore, the $\overline{\mathbf{U}}_1(\theta, \varphi, kr)$ matrix firstly introduced in Equation (5) remains identical. However, Equation (6) cannot be used as the $\overline{\mathbf{U}}_2(\mathbf{E}_i, \beta)$ matrix no longer links $\mathbf{D}$ with $\boldsymbol{\mathcal{P}}$ for a random dispersion. In short, β is no longer a degree of freedom as it is the integration variable of Equation (11).

Therefore, one needs to find a matrix $\overline{\mathbf{U}}_3(\mathbf{E}_i)$ (see Appendix F for the details) that satisfies:

$$\frac{\tilde{\boldsymbol{\mathcal{P}}}}{N} = \begin{pmatrix}\tilde{\mathcal{P}}_0\\ \tilde{\mathcal{P}}_1\\ 0\\ 0\end{pmatrix} = \begin{pmatrix}|\alpha_1|^2 + |\alpha_2|^2\\ \Re\{\alpha_1\alpha_2^*\}\\ 0\\ 0\end{pmatrix} = \overline{\mathbf{U}}_3(\mathbf{E}_i)\overline{\mathbf{U}}_1(\theta, \varphi, kr)\langle\mathbf{S}\rangle \tag{12}$$

Equation (12) links a measurement of the rotationally-averaged Stokes vector $\langle\mathbf{S}\rangle$ at a single collection angle in the far-field with the vector $\tilde{\boldsymbol{\mathcal{P}}}$. Moreover, one can note that the polarizability vector $\boldsymbol{\mathcal{P}}$, given in Equation (7) determines $\tilde{\boldsymbol{\mathcal{P}}}$. This fact implies that the polarimetry properties of a single NP at a fixed orientation angle β can be used to infer the electromagnetic properties of the same NP when this is randomly oriented. However, the converse is not true. Specifically, the term $\Im\{\alpha_1\alpha_2^*\}$ is lost in the averaging given in Equation (11), as it is associated with trigonometric functions that are odd in β and thus vanish upon integration. Moreover, one cannot determine $|\alpha_1|^2$ and $|\alpha_2|^2$ separately, a distinction that can be achieved at the single-particle level using Equation (7). In this regard, I invite the reader to read Appendix F to get more insights into the calculation of rotationally averaged quantities.

At this stage, it is important to mention that one can still determine rotationally averaged quantities using Equation (12). In particular, I will show that the rotationally averaged scattering cross-section, $\langle\sigma_{sca}\rangle$, and the rotationally averaged optical recoil torque, $\langle\boldsymbol{\Gamma}_{rec}\rangle$, can be determined from $\tilde{\boldsymbol{\mathcal{P}}}$. Indeed, performing the rotational averaging of Equations (8) and (9) yields

$$\langle\sigma_{sca}\rangle = \frac{k^4}{12\pi}\left(|\alpha_1|^2 + |\alpha_2|^2\right) = \frac{k^4}{12\pi}\tilde{\mathcal{P}}_0 = \frac{k^4}{12\pi}(\mathcal{P}_0 + \mathcal{P}_1) \tag{13}$$

$$\frac{\langle \Gamma_{\text{rec}} \rangle}{\Gamma_0} = \frac{2\Im\{E_x E_y^*\}}{|E_0|^2} \frac{\Re\{\alpha_1 \alpha_2^*\}}{V^2} = -\frac{\sigma \tilde{\mathcal{P}}_1}{V^2} = -\frac{\sigma \mathcal{P}_2}{V^2} \tag{14}$$

Here, I have introduced σ as the helicity of the incident field [75–77]. Equations (13) and (14) show that rotationally-averaged quantities such as $\langle \sigma_{\text{sca}} \rangle$ and $\langle \Gamma_{\text{rec}} \rangle$, which typically require integration techniques, can be determined from $\tilde{\boldsymbol{\mathcal{P}}}$. All that one needs to do is calculate the matrices $\overline{\mathbf{U}}_3(\mathbf{E}_{\text{i}})$ and $\overline{\mathbf{U}}_1(\theta, \varphi, kr)$ of Equation (12) to determine $\tilde{\boldsymbol{\mathcal{P}}}$. In this regard, I provide a couple of examples of $\overline{\mathbf{U}}_3(\mathbf{E}_{\text{i}})$ in Appendix F.

7 | Conclusion and Outlook

In summary, I have presented a simple, versatile, and robust polarimetry-based technique to characterize the optical response of anisotropic NPs. The method relies on a single-angle Stokes vector measurement and yields an overlooked observable: the polarizability vector $\boldsymbol{\mathcal{P}}$ given in Equation (1), which, as I showed, encodes essential information about the optical response of the NP. Importantly, I have shown that any physical quantity expressible as a combination of $\boldsymbol{\mathcal{P}}$ can be determined using Equation (7). As examples, I have expressed the scattering cross-section σ_{sca}, the optical recoil torque Γ_{rec}, and the near-field amplitude $\mathbf{E}_{\text{sca}}^{\text{NF-MF}}$ in terms of $\boldsymbol{\mathcal{P}}$. This connection reveals that the tools often required to determine σ_{sca}, Γ_{rec}, and $\mathbf{E}_{\text{sca}}^{\text{NF-MF}}$–such as an integrating sphere, a high-speed camera or quadrant photodiode, and the SMOM technique–may not be necessary. Instead, a single Stokes vector measurement at an angle of choice suffices. Moreover, I have established a connection between the polarimetric response of a single NP and that of random dispersions of identical NPs, showing that $\boldsymbol{\mathcal{P}}$ remains a meaningful observable in both scenarios.

I envision that my polarimetric technique can be further applied to probe the influence of different shells in coated NPs of various geometries, similar to what is now commonly done with the extinction cross-section. More specifically, one can use Equation (7) to determine $\boldsymbol{\mathcal{P}}$ before and after shell deposition to quantitatively assess the shell's impact on the functionalized NP [78, 79]. These sequential Stokes measurements may be employed, for instance, to investigate the role of silica–gold coated nanorods in SERS enhancements [80, 81], to explore corona protein formation on NPs [82], or to evaluate the catalytic performance of metal-coated NPs [83].

Moreover, my findings can help characterize the optical response of anisotropic NPs in other related areas of research. In particular, the Stokes polarimetry method presented in this work can aid to characterizing the optical response of anisotropic NPs attached to an AFM probe tip, which is crucial for improving the precision of the next generation of tip-enhanced nanoscopy techniques [84]. In addition, I envision that an extended version of my polarimetry method could be used to determine specific components of the second-order susceptibility tensor $\chi(2)$ in the context of second harmonic generation through far-field polarimetry measurements. In particular, by connecting $\chi(2)$ with the Stokes vector, which can potentially find applications in tissue imaging [85], and human cancer detection [86].

Acknowledgements

J.O-T. acknowledged Dr. Adrián Juan-Delgado, Dr. Antonio García-Martín, and Dr. Alejandro Manjavacas for interesting discussions and Dr. Matt Majic for the help with Figure 2. J.O-T acknowledged financial support from the Spanish Ministry of Science and Innovation (MCIN), AEI, and FEDER (UE) through projects PID2022-137569NB. J.O-T. also acknowledges MICINN for the Ramon y Cajal Fellowship (RYC2024-050342-I) and the fellowship (LCF/BQ/PR25/12110015) from "La Caixa" Foundation.

Conflicts of Interest

The authors declare no conflict of interest.

Data Availability Statement

The data that support the findings of this study are available from the corresponding author upon reasonable request.

References

1. S. A. Maier, M. L. Brongersma, P. G. Kik, S. Meltzer, A. A. Requicha, and H. A. Atwater, "Plasmonics–A Route to Nanoscale Optical Devices," *Advanced Materials* 13, no. 19 (2001): 1501–1505.

2. A. Manjavacas and F. García de Abajo, "Tunable Plasmons in Atomically Thin Gold Nanodisks," *Nature Communications* 5, no. 1 (2014): 3548.

3. F. Hao, C. L. Nehl, J. H. Hafner, and P. Nordlander, "Plasmon Resonances of a Gold Nanostar," *Nano Letters* 7, no. 3 (2007): 729–732.

4. R. E. Armstrong, M. Horávcek, and P. Zijlstra, "Plasmonic Assemblies for Real-Time Single-Molecule Biosensing," *Small* 16, no. 52 (2020): 2003934.

5. A. Al-Zubeidi, L. A. McCarthy, A. Rafiei-Miandashti, T. S. Heiderscheit, and S. Link, "Single-Particle Scattering Spectroscopy: Fundamentals and Applications," *Nanophotonics* 10, no. 6 (2021): 1621–1655.

6. D. Lin, Y. Duan, P. Bandaru, P. Li, M. S. Ansari, A. Y. Polyakov, J. Wilhelmsen, and M. P. Jonsson, "Switchable Narrow Nonlocal Conducting Polymer Plasmonics," *Nature Communications* 16, no. 1 (2025): 1–10.

7. L. A. Jakob, A. Juan-Delgado, N. S. Mueller, S. Hu, R. Arul, R. A. Boto, et al., "Optomechanical Pumping of Collective Molecular Vibrations in Plasmonic Nanocavities," *ACS Nano ACS Publications* 19, no. 11 (2025).: 10977–10988.

8. C. F. Bohren and D. R. Huffman, *Absorption and Scattering of Light by Small Particles* (John Wiley & Sons, 2008).

9. H. Chen, T. Ming, S. Zhang, Z. Jin, B. Yang, and J. Wang, "Effect of the Dielectric Properties of Substrates on the Scattering Patterns of Gold Nanorods," *Acs Nano* 5, no. 6 (2011): 4865–4877.

10. K. C. Vernon, A. M. Funston, C. Novo, D. E. Gómez, P. Mulvaney, and T. J. Davis, "Influence of Particle- Substrate Interaction on Localized Plasmon Resonances," *Nano Letters* 10, no. 6 (2010): 2080–2086.

11. M. I. Mishchenko, L. D. Travis, and A. A. Lacis, *Scattering, Absorption, and Emission of Light by Small Particles* (Cambridge University Press, 2002).

12. N. Asadova, K. Achouri, K. Arjas, et al., "T-Matrix Representation of Optical Scattering Response: Suggestion for a Data Format," *Journal of Quantitative Spectroscopy and Radiative Transfer* 333, (2025): 109310.

13. F. B. Arango and A. F. Koenderink, "Polarizability Tensor Retrieval for Magnetic and Plasmonic Antenna Design," *New Journal of Physics* 15, no. 7 (2013): 073023.

14. C. Multiphysics, "Introduction to COMSOL multiphysics®," *COMSOL Multiphysics, Burlington, MA, accessed Feb* 9, no. 2018 (1998): 32.

15. G. Mie, "Beiträge zur Optik trüber Medien, Speziell Kolloidaler Metallösungen," *Annalen der Physik* 330, no. 3 (1908): 377–445.

16. J. Olmos-Trigo, C. Sanz-Fernández, F. S. Bergeret, and J. J. Sáenz, "Asymmetry and spin-orbit coupling of light scattered from subwavelength particles," *Optics Letters* 44, no. 7 (2019): 1762–1765.

17. J. Olmos-Trigo, C. Sanz-Fernández, A. García-Etxarri, G. Molina-Terriza, F. S. Bergeret, and J. J. Sáenz, "Enhanced spin-orbit optical mirages from dual nanospheres," *Physical Review A* 99, no. 1 (2019): 013852.

18. M. Husnik, S. Linden, R. Diehl, J. Niegemann, K. Busch, and M. Wegener, "Quantitative experimental determination of scattering and absorption cross-section spectra of individual optical metallic nanoantennas," *Physical review letters* 109, no. 23 (2012): 233902.

19. W. Cao, M. Chern, A. M. Dennis, and K. A. Brown, "Measuring Nanoparticle Polarizability Using Fluorescence Microscopy," *Nano Letters* 19, no. 8 (2019): 5762–5768.

20. A. Zilli, W. Langbein, and P. Borri, "Quantitative Measurement of the Optical Cross Sections of Single Nano-Objects by Correlative Transmission and Scattering Microspectroscopy," *ACS Photonics* 6, no. 8 (2019): 2149–2160.

21. S. Khadir, D. Andrén, P. C. Chaumet, S. Monneret, N. Bonod, M. Käll, A. Sentenac, and G. Baffou, "Full Optical Characterization of Single Nanoparticles Using Quantitative Phase Imaging," *Optica* 7, no. 3 (2020): 243–248.

22. M. Mader, J. Benedikter, L. Husel, T. W. Hansch, and D. Hunger, "Quantitative Determination of the Complex Polarizability of Individual Nanoparticles by Scanning Cavity Microscopy," *ACS Photonics* 9, no. 2 (2022): 466–473.

23. Y. Park, C. Depeursinge, and G. Popescu, "Quantitative Phase Imaging in Biomedicine," *Nature Photonics* 12, no. 10 (2018): 578–589.

24. S. Hamilton, D. Regan, L. Payne, W. Langbein, and P. Borri, "Sizing Individual Dielectric Nanoparticles With Quantitative Differential Interference Contrast Microscopy," *Analyst* 147, no. 8 (2022): 1567–1580.

25. L. Priest, J. S. Peters, and P. Kukura, "Scattering-Based Light Microscopy: From Metal Nanoparticles to Single Proteins," *Chemical Reviews* 121, no. 19 (2021): 11937–11970.

26. O. Hauler, L. A. Jakob, K. Braun, F. Laible, M. Fleischer, A. J. Meixner, and F. Wackenhut, "Sensitive Interferometric Plasmon Ruler Based on a Single Nanodimer," *The Journal of Physical Chemistry C* 125, no. 11 (2021): 6486–6493.

27. L. Saemisch, N. F. Van Hulst, and M. Liebel, "One-Shot Phase Image Distinction of Plasmonic and Dielectric Nanoparticles," *Nano Letters* 21, no. 9 (2021): 4021–4028.

28. H. Lee, H. Park, G. J. Yeon, and Z. H. Kim, "Amplitude and Phase Spectra of Light Scattered From a Single Nanoparticle," *ACS Photonics* 9, no. 9 (2022): 3052–3059.

29. C. Gentner, B. Rogez, H. M. Robert, A. Aggoun, G. Tessier, P. Bon, and P. Berto, "Enhanced Quantitative Wavefront Imaging for Nano-Object Characterization," *ACS Nano* 18, no. 29 (2024): 19247–19256.

30. E. Olsén, B. García Rodríguez, F. Skärberg, P. Parkkila, G. Volpe, F. Höök, and D. Sundås Midtvedt, "Quantitative Imaging of Single Light-Absorbing Nanoparticles by Widefield Interferometric Photothermal Microscopy," *Nano Letters* 24, no. 24 (2024): 1874–1881.

31. A. Tcherniak, J. Ha, S. Dominguez-Medina, L. S. Slaughter, and S. Link, "Probing a Century old Prediction one Plasmonic Particle at a Time," *Nano Letters* 10, no. 4 (2010): 1398–1404.

32. P. Berto, E. Bermúdez Ureña, P. Bon, R. Quidant, H. Rigneault, and G. Baffou, "Quantitative Absorption Spectroscopy of Nano-Objects," *Physical Review B* 86 (2012): 165417.

33. S. D. Gennaro, Y. Sonnefraud, N. Verellen, P. Van Dorpe, V. V. Moshchalkov, S. A. Maier, and R. F. Oulton, "Spectral Interferometric Microscopy Reveals Absorption by Individual Optical Nanoantennas From Extinction Phase," *Nature Communications* 5, no. 1 (2014): 3748.

34. S. A. Mann, B. Sciacca, Y. Zhang, J. Wang, E. Kontoleta, H. Liu, and E. C. Garnett, "Integrating Sphere Microscopy for Direct Absorption Measurements of Single Nanostructures," *ACS Nano* 11, no. 2 (2017): 1412–1418.

35. J. Grand, B. Auguié, and E. C. Le Ru, "Combined Extinction and Absorption UV–Visible Spectroscopy as a Method for Revealing Shape Imperfections of Metallic Nanoparticles," *Analytical Chemistry* 91, no. 22 (2019): 14639–14648.

36. Y.-C. Huang, T.-H. Chen, J.-Y. Juo, S.-W. Chu, and C.-L. Hsieh, "Quantitative Imaging of Single Light-Absorbing Nanoparticles by Widefield Interferometric Photothermal Microscopy," *ACS Photonics* 8, no. 2 (2021): 592–602.

37. F. Alabdullah, V. Singh, L. Payne, et al., "Radially Polarized Light in Single Particle Optical Extinction Microscopy Identifies Silver Nanoplates," *Applied Physics Letters* 124, no. 18 (2024).

38. J. R. Deop-Ruano and A. Manjavacas, "Thermal Radiation Force and Torque on Moving Nanostructures With Anisotropic Optical Response," *Physical Review Letters* 134, no. 11 (2025): 113604.

39. J. D. Jackson, "Nanophotonic Platforms for Enhanced Chiral Sensing," *Classical Electrodynamics* (John Wiley & Sons, New York, 1999).

40. A. Mildner, A. Horrer, P. Weiss, et al., "Decoding Polarization in a Single Achiral Gold Nanostructure From Emitted Far-Field Radiation," *ACS Nano* 17, no. 24 (2023): 25656–25666.

41. Y. Cui, Y. Chen, J. Li, et al., "Mode-Dependent Far-Field Radiation of Circularly Polarized Light by a Single Plasmonic Nanohelix," *Advanced Optical Materials* 13, no. 8 (2025): 2402704.

42. J. Lasa-Alonso, I. Gómez-Viloria, A. Nodar, A. García-Etxarri, G. Molina-Terriza, and J. Olmos-Trigo, "Characterizing Cylindrical Particles Upon Local Measurements of Two Stokes Parameters," *Characterizing cylindrical particles upon local measurements of two stokes parameters* (2023), http://arxiv.org/abs/2304.02762.

43. J. Olmos-Trigo, "Solving Maxwell's Equations Using Polarimetry Alone," *Nano Letters* 24, no. 28 (2024): 8658–8663.

44. M. Gauchet, F. Perrier, C. Bonnet, et al., "Bright-Field Polarimetry of a Single Plasmonic Nanostructure Combining Polarization and Position Modulation Techniques," *ACS Photonics* 12, no. 7(2025).: 3856–3870.

45. J. Olmos-Trigo, "Revealing the Electric and Magnetic Nature of the Scattered Light," *ACS Photonics* 11, no. 9 (2024): 3697–3703.

46. P. Zijlstra, J. W. Chon, and M. Gu, "Five-Dimensional Optical Recording Mediated by Surface Plasmons in Gold Nanorods," *Nature* 459, no. 7245 (2009): 410–413.

47. W. Ahmed, E. S. Kooij, A. Van Silfhout, and B. Poelsema, "Quantitative Analysis of Gold Nanorod Alignment After Electric Field-Assisted Deposition," *Nano Letters* 9, no. 11 (2009): 3786–3794.

48. L. Shao, Z.-J. Yang, D. Andrén, P. Johansson, and M. Kall, "Gold Nanorod Rotary Motors Driven by Resonant Light Scattering," *ACS Nano* 9, no. 12 (2015): 12542–12551.

49. P. Zijlstra, M. van Stee, N. Verhart, Z. Gu, and M. Orrit, "Rotational Diffusion and Alignment of Short Gold Nanorods in an External Electric Field," *Physical Chemistry Chemical Physics* 14, no. 13 (2012): 4584–4588.

50. J. A. Rodrigo, T. Alieva, V. Manzaneda-González, and A. Guerrero-Martínez, "All-Optical Trapping and Programmable Transport of Gold Nanorods with Simultaneous Orientation and Spinning Control," *ACS Nano* 18, no. 40 (2024): 27738–27751.

51. P. C. Simo, A. Mildner, D. P. Kern, and M. Fleischer, "Dipole Determination by Polarimetric Spectroscopy Yielding the Orientation of Gold Nanorods," *Small Science* 5, no. 6 (2025): 2400340.

52. J. Olmos-Trigo, M. Nieto-Vesperinas, and G. Molina-Terriza, "Spheres of Maximum Electromagnetic Chirality," *Physical Review Research* 6, no. 4 (2024): 043192.

53. W. Ni, X. Kou, Z. Yang, and J. Wang, "Tailoring Longitudinal Surface Plasmon Wavelengths, Scattering and Absorption Cross Sections of Gold Nanorods," *ACS Nano* 2, no. 4 (2008): 677–686.

54. J. Zheng, X. Cheng, H. Zhang, X. Bai, R. Ai, L. Shao, and J. Wang, "Gold Nanorods: the Most Versatile Plasmonic Nanoparticles," *Chemical Reviews* 121, no. 21 (2021): 13342–13453.

55. W. Ye, "Nonlocal Optical Response of Particle Plasmons in Single Gold Nanorods," *Nano Letters* 23, no. 16 (2023): 7658–7664.

56. K. Trofymchuk, K. Kołataj, V. Glembockyte, F. Zhu, G. P. Acuna, T. Liedl, and P. Tinnefeld, "Gold Nanorod DNA Origami Antennas for 3 Orders of Magnitude Fluorescence Enhancement in NIR," *ACS Nano* 17, no. 2 (2023): 1327–1334.

57. Y. Yin, A. A. Trichet, J. Qian, and J. M. Smith, "Shape Measurement of Single Gold Nanorods in Water Using Open-Access Optical Microcavities," *The Journal of Physical Chemistry Letters* 15, no. 49 (2024): 12105–12111.

58. Y. Yang, W. Jung, et al., "Angle-Resolved Polarimetry With Quasi-Bound States in the Continuum Plasmonic Metamaterials via 3D Aerosol Nanoprinting," *ACS Nano* 18, no. 20 (2024): 12771–12780.

59. P. Bouchal, P. Dvorak, M. Hrton, K. Rovenska, R. Chmelik, T. Sikola, and Z. Bouchal, "Angle-Resolved Polarimetry With Quasi-Bound States in the Continuum Plasmonic Metamaterials via 3D Aerosol Nanoprinting," *ACS Photonics* 10, no. 9 (2023): 3331–3341.

60. Z. J. O'Dell, M. Knobeloch, S. E. Skrabalak, and K. A. Willets, "High-Throughput All-Optical Determination of Nanorod Size and Orientation," *Nano Letters* 24, no. 24 (2024): 7269–7275.

61. T. Fordey, P. Bouchal, P. Schovánek, et al., "Angle-Resolved Polarimetry With Quasi-Bound States in the Continuum Plasmonic Metamaterials via 3D Aerosol Nanoprinting," *Nano Letters* 21, no. 17 (2021): 7244–7251.

62. N. G. Khlebtsov and S. V. Zarkov, "Analytical Modeling of Coated Plasmonic Particles," *The Journal of Physical Chemistry C* 128, no. 36 (2024): 15029–15040.

63. M. Majic, L. Pratley, D. Schebarchov, W. R. Somerville, B. Auguié, and E. C. Le Ru, "Approximate T Matrix and Optical Properties of Spheroidal Particles to Third Order With Respect to Size Parameter," *Physical Review A* 99, no. 1 (2019): 013853.

64. M. R. Majić, B. Auguié, and E. C. Le Ru, "Comparison of Dynamic Corrections to the Quasistatic Polarizability and Optical Properties of Small Spheroidal Particles," *The Journal of Chemical Physics* 156, no. 10 (2022): 104110.

65. This infeasibility stems from the fact that $|\alpha_1|^2$ and $|\alpha_2|^2$ typically emerge additively in σ_{sca}.

66. P. L. Marston and J. H. Crichton, "Radiation torque on a sphere caused by a circularly-polarized electromagnetic," *Physical Review A* 30, no. 5 (1984): 2508.

67. J. Barton, D. Alexander, and S. Schaub, "Theoretical Determination of net Radiation Force and Torque for a Spherical Particle Illuminated by a Focused Laser Beam," *Journal of Applied Physics* 66, no. 10 (1989): 4594–4602.

68. M. Nieto-Vesperinas, "Optical torque: Electromagnetic spin and orbital-angular-momentum conservation laws and their significance," *Physical Review A* 92, no. 4 (2015): 043843.

69. M. Riccardi and O. J. Martin, "Electromagnetic Forces and Torques: From Dielectrophoresis to Optical Tweezers," *Chemical Reviews* 123, no. 4 (2023): 1680–1711.

70. X. Xu, M. Nieto-Vesperinas, Y. Zhou, et al., "Gradient and Curl Optical Torques," *Nature Communications* 15, no. 1 (2024): 6230.

71. H. Chen, L. Feng, J. Ma, C. Liang, Z. Lin, and H. Zheng, "Left-Handed Optical Torque on Dipolar Plasmonic Nanoparticles Induced by Fano-Like Resonance," *Physical Review B* 106, no. 5 (2022): 054301.

72. T. Qi, F. Han, W. Liu, and Z. Yan, "Stable Negative Optical Torque in Optically Bound Nanoparticle Dimers," *Nano Letters* 22, no. 21 (2022): 8482–8486.

73. J. Wen, H. Chen, H. Zheng, et al., "Optical Intensity-Gradient Torque due to Chiral Multipole Interplay," *arXiv preprint arXiv:2409.11924* (2024).

74. I. Toftul, M. Petrov, R. Quidant, and Y. Kivshar, "Optical Supertorque Induced by Mie-Resonant Modes," *ACS Photonics* 12, no. 7, (2025): 3447–3456.

75. J. Olmos-Trigo, D. R. Abujetas, C. Sanz-Fernández, et al., "Unveiling Dipolar Spectral Regimes of Large Dielectric Mie Spheres From Helicity Conservation," *Physical Review Research* 2, no. 4 (2020): 043021.

76. J. Olmos-Trigo, D. R. Abujetas, C. Sanz-Fernández, J. A. Sánchez-Gil, and J. J. Sáenz, "Optimal Backward Light Scattering by Dipolar Particles," *Physical Review Research* 2, no. 1 (2020): 013225.

77. J. Olmos Trigo, C. Sanz-Fernández, and I. Fernandez-Corbaton, "A Novel Chiroptical Spectroscopy Technique," *arXiv e-prints* (2025): 2509.

78. N. Siegel, H. Hasebe, G. Chiarelli, et al., "Universal Click-Chemistry Approach for the DNA Functionalization of Nanoparticles," *Journal of the American Chemical Society* 146, no. 25 (2024): 17250–17260.

79. F. Stete, W. Koopman, C. Henkel, O. Benson, G. Kewes, and M. Bargheer, "Optical Spectra of Plasmon–Exciton Core–Shell Nanoparticles: A Heuristic Quantum Approach," *ACS Photonics* 10, no. 8 (2023): 2511–2520.

80. M. J. Kim, D. H. Jung, C. Y. Lee, S. Hong, J. H. Heo, and J. H. Lee, "Structurally Engineered Silica Shells on Gold Nanorods for Biomedical Applications," *Small Structures* 4, no. 9 (2023): 2300047.

81. S. M. Meyer and C. J. Murphy, "Anisotropic Silica Coating on Gold Nanorods Boosts Their Potential as SERS Sensors," *Nanoscale* 14, no. 13 (2022): 5214–5226.

82. M. Dolci, Y. Wang, S. W. Nooteboom, P. E. D. Soto Rodriguez, S. Sanchez, L. Albertazzi, and P. Zijlstra, "Real-Time Optical Tracking of Protein Corona Formation on Single Nanoparticles in Serum," *ACS Nano* 17, no. 20 (2023): 20167–20178.

83. B. Li, T. Gu, T. Ming, et al., "(Gold Core)@(Ceria Shell) Nanostructures for Plasmon-Enhanced Catalytic Reactions Under Visible Light," *Acs Nano* 8, no. 8 (2014): 8152–8162.

84. J. Belhassen, S. Glass, E. Teblum, G. A. Stanciu, D. E. Tranca, Z. Zalevsky, S. G. Stanciu, and A. Karsenty, "Toward Augmenting Tip-Enhanced Nanoscopy With Optically Resolved Scanning Probe Tips," *Advanced Photonics Nexus* 2, no. 2 (2023): 026002–026002.

85. V. N. Astratov, Y. B. Sahel, Y. C. Eldar, et al., "Roadmap on Label-Free Super-Resolution Imaging," *Laser & Photonics Reviews* 17, no. 12 (2023): 2200029.

86. K. R. Campbell, R. Chaudhary, J. M. Handel, M. S. Patankar, and P. J. Campagnola, "Polarization-Resolved Second Harmonic Generation Imaging of Human Ovarian Cancer," *Journal of Biomedical Optics* 23, no. 6 (2018): 066501–066501.

Appendix A: Derivation of the $\overline{\mathbf{U}}_1(\theta, \varphi, kr)$ Matrix

In this section, I derive the $\overline{\mathbf{U}}_1(\theta, \varphi, kr)$ matrix introduced in Equation (5) of the main text. This matrix relates the Stokes vector $\mathbf{S}$ with the dipolar vector $\mathbf{D}$. I start by writing the Stokes vector as a function of the induced electric-point dipole $\mathbf{p}$ [39]:

$$s_0 = G_0\left[|p_\theta|^2 + |p_\varphi|^2\right], \qquad s_1 = G_0\left[|p_\theta|^2 - |p_\varphi|^2\right], \qquad s_2 = -2G_0\Re\{p_\theta p_\varphi^*\}, \qquad s_3 = 2G_0\Im\{p_\theta p_\varphi^*\} \tag{A1}$$

Here, I have defined $G_0 = (k^2/(4\pi r\epsilon_h\epsilon_0))^2$. Now, any vector in spherical coordinates satisfies:

$$p_\theta = \cos\theta\left(p_x\cos\varphi + p_y\sin\varphi\right) - p_z\sin\theta, \qquad p_\varphi = p_y\cos\varphi - p_x\sin\varphi \tag{A2}$$

Expanding Equation (A1) using Equation (A2) for $p_z = 0$, one has

$$\begin{pmatrix} s_0 \\ s_1 \\ s_2 \\ s_3 \end{pmatrix} = G_0 \begin{pmatrix} \cos^2\theta\cos^2\varphi + \sin^2\varphi & \cos^2\theta\sin^2\varphi + \cos^2\varphi & \sin 2\varphi(\cos^2\theta - 1) & 0 \\ \cos^2\theta\cos^2\varphi - \sin^2\varphi & \cos^2\theta\sin^2\varphi - \cos^2\varphi & \sin 2\varphi(\cos^2\theta + 1) & 0 \\ \cos\theta\sin 2\varphi & -\cos\theta\sin 2\varphi & -2\cos\theta\cos 2\varphi & 0 \\ 0 & 0 & 0 & 2\cos\theta \end{pmatrix} \begin{pmatrix} |p_x|^2 \\ |p_y|^2 \\ \Re\{p_x p_y^*\} \\ \Im\{p_x p_y^*\} \end{pmatrix}. \tag{A3}$$

To obtain the $\overline{\mathbf{U}}_1(\theta, \varphi, kr)$ matrix, I need to invert Equation (A3). However, certain angles make such inversion unfeasible. For instance, the scattering angle $\theta = \pi/2$ makes such a matrix singular. Having noted this fact, I invert Equation (A3), yielding

$$\begin{pmatrix} |p_x|^2 \\ |p_y|^2 \\ \Re\{p_x p_y^*\} \\ \Im\{p_x p_y^*\} \end{pmatrix} = \frac{1}{8G_0} \begin{pmatrix} 2\left(1 + \sec^2\theta + \cos 2\varphi\tan^2\theta\right) & (3 + \cos 2\theta)\cos 2\varphi\sec^2\theta + 2\tan^2\theta & 4\sec\theta\sin 2\varphi & 0 \\ 2\left(1 + \sec^2\theta - \cos 2\varphi\tan^2\theta\right) & -(3 + \cos 2\theta)\cos 2\varphi\sec^2\theta + 2\tan^2\theta & -4\sec\theta\sin 2\varphi & 0 \\ 2\tan^2\theta\sin 2\varphi & 2(1 + \sec^2\theta)\sin 2\varphi & -4\sec\theta\cos 2\varphi & 0 \\ 0 & 0 & 0 & 4\sec\theta \end{pmatrix} \begin{pmatrix} s_0 \\ s_1 \\ s_2 \\ s_3 \end{pmatrix}. \tag{A4}$$

Inspecting Equation (A4), one can realize that the $\overline{\mathbf{U}}_1(\theta, \varphi, kr)$ matrix is:

$$\overline{\mathbf{U}}_1(\theta, \varphi, kr) = \frac{1}{8G_0} \begin{pmatrix} 2\left(1 + \sec^2\theta + \cos 2\varphi\tan^2\theta\right) & (3 + \cos 2\theta)\cos 2\varphi\sec^2\theta + 2\tan^2\theta & 4\sec\theta\sin 2\varphi & 0 \\ 2\left(1 + \sec^2\theta - \cos 2\varphi\tan^2\theta\right) & -(3 + \cos 2\theta)\cos 2\varphi\sec^2\theta + 2\tan^2\theta & -4\sec\theta\sin 2\varphi & 0 \\ 2\tan^2\theta\sin 2\varphi & 2(1 + \sec^2\theta)\sin 2\varphi & -4\sec\theta\cos 2\varphi & 0 \\ 0 & 0 & 0 & 4\sec\theta \end{pmatrix}. \tag{A5}$$

Appendix B: Derivation of the $\overline{\mathbf{U}}_2(\mathbf{E}_\mathrm{i}, \beta)$ Matrix

In this section, I derive the $\overline{\mathbf{U}}_2(\mathbf{E}_\mathrm{i}, \beta)$ matrix introduced in Equation (6), which relates the dipolar vector $\mathbf{D}$ and the polarizability vector $\boldsymbol{\mathcal{P}}$. To obtain $\overline{\mathbf{U}}_2(\mathbf{E}_\mathrm{i}, \beta)$, I first express p_x and p_y as functions of α_1 and α_2 and the orientation angle β. Expanding Equation (2) using Equation (3) of the main text yields

$$\frac{p_x}{\epsilon_h\epsilon_0} = (\alpha_1\cos^2\beta + \alpha_2\sin^2\beta)E_x + (\alpha_1 - \alpha_2)\cos\beta\sin\beta E_y \tag{B1}$$

$$\frac{p_y}{\epsilon_h\epsilon_0} = (\alpha_1 - \alpha_2)\cos\beta\sin\beta E_x + (\alpha_1\sin^2\beta + \alpha_2\cos^2\beta)E_y \tag{B2}$$

Manipulating Equations (B1)-(B2), yields

$$\begin{aligned}\left|\frac{p_x}{\epsilon_h\epsilon_0}\right|^2 =& |\alpha_1|^2\cos^2\beta\left(|E_x|^2\cos^2\beta + |E_y|^2\sin^2\beta + \Re\{E_xE_y^*\}\sin 2\beta\right) + |\alpha_2|^2\sin^2\beta\left(|E_x|^2\sin^2\beta + |E_y|^2\cos^2\beta - \Re\{E_xE_y^*\}\sin 2\beta\right) \\ &+\Re\{\alpha_1\alpha_2^*\}\sin 2\beta\left[\sin\beta\cos\beta\left(|E_x|^2 - |E_y|^2\right) - \Re\{E_xE_y^*\}\cos 2\beta\right] + \Im\{\alpha_1\alpha_2^*\}\Im\{E_xE_y^*\}\sin 2\beta,\end{aligned} \tag{B3}$$

$$\begin{aligned}\left|\frac{p_y}{\epsilon_h\epsilon_0}\right|^2 =& |\alpha_1|^2\sin^2\beta\left(|E_y|^2\sin^2\beta + |E_x|^2\cos^2\beta + \Re\{E_xE_y^*\}\sin 2\beta\right) + |\alpha_2|^2\cos^2\beta\left(|E_y|^2\cos^2\beta + |E_x|^2\sin^2\beta - \Re\{E_xE_y^*\}\sin 2\beta\right) \\ &+\Re\{\alpha_1\alpha_2^*\}\sin 2\beta\left[\sin\beta\cos\beta\left(|E_y|^2 - |E_x|^2\right) + \Re\{E_xE_y^*\}\cos 2\beta\right] - \Im\{\alpha_1\alpha_2^*\}\Im\{E_xE_y^*\}\sin 2\beta,\end{aligned} \tag{B4}$$

$$\begin{aligned}\frac{\Re\{p_xp_y^*\}}{(\epsilon_h\epsilon_0)^2} =& \sin\beta\cos\beta\left(|\alpha_1|^2\left(|E_x|^2\cos^2\beta + |E_y|^2\sin^2\beta + \Re\{E_xE_y^*\}\sin 2\beta\right) - |\alpha_2|^2\left(|E_x|^2\sin^2\beta + |E_y|^2\cos^2\beta - \Re\{E_xE_y^*\}\sin 2\beta\right)\right) \\ &+\Re\{\alpha_1\alpha_2^*\}\cos 2\beta\left(\left(|E_y|^2 - |E_x|^2\right)\sin\beta\cos\beta + \Re\{E_xE_y^*\}\cos 2\beta\right) - \Im\{\alpha_1\alpha_2^*\}\Im\{E_xE_y^*\}\cos 2\beta,\end{aligned} \tag{B5}$$

$$\frac{\Im\{p_xp_y^*\}}{(\epsilon_h\epsilon_0)^2} = \Re\{\alpha_1\alpha_2^*\}\Im\{E_xE_y^*\} + \Im\{\alpha_1\alpha_2^*\}\left(\sin\beta\cos\beta\left(|E_y|^2 - |E_x|^2\right) + \Re\{E_xE_y^*\}\cos 2\beta\right). \tag{B6}$$

Interestingly, one can compactly write the previous expressions as

$$\begin{pmatrix} |\alpha_1|^2 \\ |\alpha_2|^2 \\ \Re\{\alpha_1\alpha_2^*\} \\ \Im\{\alpha_1\alpha_2^*\} \end{pmatrix} = \overline{\mathbf{U}}_2(\mathbf{E}_\mathrm{i},\beta)\begin{pmatrix} |p_x|^2 \\ |p_y|^2 \\ \Re\{p_x p_y^*\} \\ \Im\{p_x p_y^*\} \end{pmatrix} = \frac{1}{(\epsilon_h\epsilon_0)^2}\begin{pmatrix} A_{11} & A_{12} & A_{13} & A_{14} \\ A_{21} & A_{22} & A_{23} & A_{24} \\ A_{31} & A_{32} & A_{33} & A_{34} \\ A_{41} & A_{42} & A_{43} & A_{44} \end{pmatrix}^{-1}\begin{pmatrix} |p_x|^2 \\ |p_y|^2 \\ \Re\{p_x p_y^*\} \\ \Im\{p_x p_y^*\} \end{pmatrix} = \frac{\overline{A}^{-1}(\mathbf{E}_\mathrm{i},\beta)}{(\epsilon_h\epsilon_0)^2}\begin{pmatrix} |p_x|^2 \\ |p_y|^2 \\ \Re\{p_x p_y^*\} \\ \Im\{p_x p_y^*\} \end{pmatrix} \tag{B7}$$

where the matrix elements A_{ij} are given by:

$$A_{11} = \cos^2\beta\Big(|E_x|^2\cos^2\beta + |E_y|^2\sin^2\beta + \Re\{E_xE_y^*\}\sin 2\beta\Big), \qquad A_{12} = \sin^2\beta\Big(|E_x|^2\sin^2\beta + |E_y|^2\cos^2\beta - \Re\{E_xE_y^*\}\sin 2\beta\Big),$$

$$A_{13} = \sin 2\beta\big[\sin\beta\cos\beta(|E_x|^2 - |E_y|^2) - \Re\{E_xE_y^*\}\cos 2\beta\big], \qquad A_{14} = \Im\{E_xE_y^*\}\sin 2\beta,$$

$$A_{21} = \sin^2\beta\Big(|E_y|^2\sin^2\beta + |E_x|^2\cos^2\beta + \Re\{E_xE_y^*\}\sin 2\beta\Big), \qquad A_{22} = \cos^2\beta\Big(|E_y|^2\cos^2\beta + |E_x|^2\sin^2\beta - \Re\{E_xE_y^*\}\sin 2\beta\Big),$$

$$A_{23} = \sin 2\beta\big[\sin\beta\cos\beta(|E_y|^2 - |E_x|^2) + \Re\{E_xE_y^*\}\cos 2\beta\big], \qquad A_{24} = -\Im\{E_xE_y^*\}\sin 2\beta,$$

$$A_{31} = \sin\beta\cos\beta\Big(|E_x|^2\cos^2\beta + |E_y|^2\sin^2\beta + \Re\{E_xE_y^*\}\sin 2\beta\Big), \qquad A_{32} = -\sin\beta\cos\beta\Big(|E_x|^2\sin^2\beta + |E_y|^2\cos^2\beta - \Re\{E_xE_y^*\}\sin 2\beta\Big),$$

$$A_{33} = \cos 2\beta\big[\sin\beta\cos\beta(|E_y|^2 - |E_x|^2) + \Re\{E_xE_y^*\}\cos 2\beta\big], \qquad A_{34} = -\Im\{E_xE_y^*\}\cos 2\beta,$$

$$A_{41} = 0, \qquad A_{42} = 0,$$

$$A_{43} = \Im\{E_xE_y^*\}, \qquad A_{44} = \sin\beta\cos\beta(|E_y|^2 - |E_x|^2) + \Re\{E_xE_y^*\}\cos 2\beta.$$

This completes the derivation of the $\overline{\mathbf{U}}_2(\mathbf{E}_\mathrm{i},\beta) = \overline{A}^{-1}(\mathbf{E}_\mathrm{i},\beta)/(\epsilon_h\epsilon_0)^2$ matrix, which establishes the relationship between the dipolar vector $\mathbf{D}$ and the polarizability vector $\boldsymbol{\mathcal{P}}$. There are certain combinations of $\mathbf{E}_\mathrm{i}$ and β that make $\overline{A}(\mathbf{E}_\mathrm{i},\beta)$ singular. Fortunately, these combinations can be identified in advance, both analytically and numerically, and should be avoided.

Appendix C: Reconstructing the Scattering Cross-Section Produced by an Anisotropic Dipolar NP From a Single Measurement of the Stokes Vector

In this section, I express the scattering cross-section σ_sca in terms of the polarizability vector $\boldsymbol{\mathcal{P}}$, which, in turn, is derived from the Stokes vector $\mathbf{S}$. Expanding Equation (8) of the main text using Equations (B1)–(B2), one arrives at

$$\sigma_\mathrm{sca} = \frac{k^4}{6\pi|\mathbf{E}_\mathrm{i}|^2}\Big(|\alpha_1|^2\Big(|E_x|^2\cos^2\beta + |E_y|^2\sin^2\beta + \Re\{E_xE_y^*\}\sin 2\beta\Big) + |\alpha_2|^2\Big(|E_x|^2\sin^2\beta + |E_y|^2\cos^2\beta - \Re\{E_xE_y^*\}\sin 2\beta\Big)\Big). \tag{C1}$$

One can write this expression in terms of the components of $\mathbf{P} = [\mathcal{P}_0,\mathcal{P}_1,\mathcal{P}_2,\mathcal{P}_3] = [|\alpha_1|^2, |\alpha_2|^2, \Re\{\alpha_1\alpha_2^*\}, \Im\{\alpha_1\alpha_2^*\}]$ as

$$\sigma_\mathrm{sca} = \frac{k^4}{6\pi|\mathbf{E}_\mathrm{i}|^2}\Big(\mathcal{P}_0\Big(|E_x|^2\cos^2\beta + |E_y|^2\sin^2\beta + \Re\{E_xE_y^*\}\sin 2\beta\Big) + \mathcal{P}_1\Big(|E_x|^2\sin^2\beta + |E_y|^2\cos^2\beta - \Re\{E_xE_y^*\}\sin 2\beta\Big)\Big). \tag{C2}$$

Equation C2 shows that the scattering cross-section can be derived from $\boldsymbol{\mathcal{P}}$ for any electromagnetic field $\mathbf{E}_\mathrm{i}$ and orientation angle β of the NP. To illustrate this, I show now the two examples corresponding to Table 1 of the main text along with an extra example.

i) Circularly polarized (CP) light. For an incident field $\mathbf{E}_\mathrm{i} = E_0(1,\mathrm{i})/\sqrt{2}$, Equation (C2) becomes

$$\sigma_\mathrm{sca}^\mathrm{CP} = \frac{k^4}{12\pi}\big(|\alpha_1|^2 + |\alpha_2|^2\big) = \frac{k^4}{12\pi}(\mathcal{P}_0 + \mathcal{P}_1) \tag{C3}$$

ii) Linearly polarized (LP) light. For an incident field $\mathbf{E}_\mathrm{i} = (0,E_0)$, Equation (C2) becomes

$$\sigma_\mathrm{sca}^\mathrm{LP} = \frac{k^4}{6\pi}\Big(|\alpha_1|^2\sin^2\beta + |\alpha_2|^2\cos^2\beta\Big) = \frac{k^4}{6\pi}\Big(\mathcal{P}_0\sin^2\beta + \mathcal{P}_1\cos^2\beta\Big) \tag{C4}$$

iii) Elliptically polarized (EP) light. For an incident field $\mathbf{E}_\mathrm{i} = (2,e^{i\pi/3})/\sqrt{5}$, Equation (C2) yields

$$\sigma_\mathrm{sca}^\mathrm{EP} = \frac{k^4}{30\pi}\Big(\mathcal{P}_0\Big(4\cos^2\beta + \sin^2\beta + \sin 2\beta\Big) + \mathcal{P}_1\Big(4\cos^2\beta + \sin^2\beta - \sin 2\beta\Big)\Big) \tag{C5}$$

As anticipated, $\sigma_\mathrm{sca}^\mathrm{EP}$ can be determined from the polarizability vector $\boldsymbol{\mathcal{P}}$, even if $\boldsymbol{\mathcal{P}}$ itself was not obtained using elliptically polarized light.

Appendix D: Reconstructing the Recoil Optical Torque Produced by any Anisotropic Np from A Measurement of the Stokes Vector

In this section, I express the recoil optical torque Γ_{rec} in terms of the polarizability vector $\boldsymbol{\mathcal{P}}$, which, in turn, is derived from the Stokes vector $\mathbf{S}$. The recoil optical torque Γ_{rec} induced in a NP described as electric-point dipole $\mathbf{p}$ is given by [66]

$$\Gamma_{\text{rec}} = \frac{k^3}{12\pi\epsilon_h\epsilon_0}\Im\{\mathbf{p}\times\mathbf{p}^*\}. \tag{D1}$$

Expanding Equation (D1) using Equations (2) and (3) of the main text I have

$$\Gamma_{\text{rec}} = \frac{k^3}{6\pi\epsilon_h\epsilon_0}\Im\{p_x p_y^*\} = \frac{k^3}{6\pi}\left(\Re\{\alpha_1\alpha_2^*\}\Im\{E_x E_y^*\} + \Im\{\alpha_1\alpha_2^*\}\left(\sin\beta\cos\beta\left(|E_y|^2 - |E_x|^2\right) + \Re\{E_x E_y^*\}\cos 2\beta\right)\right)\epsilon_h\epsilon_0. \tag{D2}$$

Note that I have used that $p_z = E_z = 0$. Equation D2 shows that Γ_{rec} can be derived from $\boldsymbol{\mathcal{P}}$ for any electromagnetic field $\mathbf{E}_{\text{i}}$ and orientation angle β of the NP. To illustrate this, I show now the two examples corresponding to Table 1 of the main text along with an extra example.

i) Circularly polarized (CP) light. Expanding Equation (D2) for an incident field $\mathbf{E}_{\text{i}} = E_0(1, \text{i})/\sqrt{2}$, yields

$$\frac{\Gamma_{\text{rec}}^{\text{CP}}}{\Gamma_0} = \frac{\Re\{\alpha_1\alpha_2^*\}}{V^2} = \frac{\mathcal{P}_2}{V^2}, \qquad \text{with} \qquad \Gamma_0 = \frac{k^3|E_0|^2\epsilon_h\epsilon_0 V^2}{12\pi} \tag{D3}$$

ii) Linearly polarized (LP) light. Expanding Equation (D2) for an incident field $\mathbf{E}_{\text{i}} = E_0(0, 1)$, yields

$$\frac{\Gamma_{\text{rec}}^{\text{LP}}}{\Gamma_0} = \frac{\Im\{\alpha_1\alpha_2^*\}\sin 2\beta}{V^2} = \frac{\mathcal{P}_3\sin 2\beta}{V^2} \tag{D4}$$

iii) Special case at $\beta = \pi/2$. Evaluating Equation (D1) at $\beta = \pi/2$ yields

$$\Gamma_{\text{rec}}^{\beta=\pi/2} = \frac{k^3}{6\pi}\left(\Re\{\alpha_1\alpha_2^*\}\Im\{E_x E_y^*\} - \Im\{\alpha_1\alpha_2^*\}\Re\{E_x E_y^*\}\right)\epsilon_h\epsilon_0 = \frac{k^3}{6\pi}\left(\mathcal{P}_2\Im\{E_x E_y^*\} - \mathcal{P}_3\Re\{E_x E_y^*\}\right)\epsilon_h\epsilon_0 \tag{D5}$$

Interestingly, this latter case does not correspond to the orientation angles β in Table 1. As explained in the main text, the recoil optical torque can still be obtained from $\boldsymbol{\mathcal{P}}$.

Appendix E: Reconstructing the Near-Field Produced by Any Anisotropic NP From a Measurement of the Stokes Vector

In this section, I show that the NF produced an anisotropic NP can be reconstructed from a single measurement of the Stokes vector $\mathbf{S}$. The amplitude of the NF produced by a electric-point dipole $\mathbf{p}$ is given by (see Equation (10) of the main text):

$$|\mathbf{E}_{\text{sca}}^{\text{NF}}|^2 = \frac{1+(kr)^2}{(4\pi r^3\epsilon_h\epsilon_0)^2}\left(4|p_r|^2 + |p_\theta|^2 + |p_\varphi|^2\right) \tag{E1}$$

where

$$|p_r|^2 = \sin^2\theta\left[|p_x|^2\cos^2\phi + |p_y|^2\sin^2\phi + 2\text{Re}\{p_x p_y^*\}\cos\phi\sin\phi\right] \tag{E2}$$

$$|p_\theta|^2 = \cos^2\theta\left[|p_x|^2\cos^2\phi + |p_y|^2\sin^2\phi + 2\text{Re}\{p_x p_y^*\}\cos\phi\sin\phi\right] \tag{E3}$$

$$|p_\varphi|^2 = |p_x|^2\sin^2\phi + |p_y|^2\cos^2\phi - 2\text{Re}\{p_x p_y^*\}\cos\phi\sin\phi \tag{E4}$$

Note that in Equations (E2)–(E4) I have assumed $p_z = 0$. Now, expanding Equation (E1) using Equations (E2)–(E4) yields

$$|\mathbf{E}_{\text{sca}}^{\text{NF}}|^2 = \frac{1+(kr)^2}{(4\pi r^3\epsilon_h\epsilon_0)^2}\left(|p_x|^2\left[1+3\sin^2\theta\cos^2\phi\right] + |p_y|^2\left[1+3\sin^2\theta\sin^2\phi\right] + 6\text{Re}\{p_x p_y^*\}\sin^2\theta\cos\phi\sin\phi\right). \tag{E5}$$

One can express this scattered field in terms of $\mathbf{D} = [D_0, D_1, D_2, D_3]^{\intercal} = [|p_x|^2, |p_y|^2, \text{Re}\{p_x p_y^*\}, \text{Im}\{p_x p_y^*\}]^{\intercal}$ as

$$|\mathbf{E}_{\text{sca}}^{\text{NF}}|^2 = \frac{1+(kr)^2}{(4\pi r^3\epsilon_h\epsilon_0)^2}\left(D_0\left[1+3\sin^2\theta\cos^2\phi\right] + D_1\left[1+3\sin^2\theta\sin^2\phi\right] + 6D_2\sin^2\theta\cos\phi\sin\phi\right) \tag{E6}$$

Since Equation (E6) only depends on $\mathbf{D}$ and simple analytical functions of $\mathbf{r}$, one can use the Stokes vector to reconstruct the scattered field produced by $\mathbf{p}$ in the near-zone. Note that one can further use the $\overline{\mathbf{U}}_2(\mathbf{E}_{\text{i}}, \beta)$ matrix to express Equation (E6) in terms of $\boldsymbol{\mathcal{P}}$.

Appendix F: Derivation of the $\overline{\mathbf{U}}_3(\mathbf{E}_\mathrm{i})$ Matrix

In this section, I derive the $\overline{\mathbf{U}}_3(\mathbf{E}_\mathrm{i})$ matrix introduced in Equation (12) of the main text. For clarity, I now rewrite Equation (12) as

$$\frac{\tilde{\boldsymbol{\mathcal{P}}}}{N} = \begin{pmatrix} \tilde{\mathcal{P}}_0 \\ \tilde{\mathcal{P}}_1 \\ 0 \\ 0 \end{pmatrix} = \begin{pmatrix} |\alpha_1|^2 + |\alpha_2|^2 \\ \Re\{\alpha_1\alpha_2^*\} \\ 0 \\ 0 \end{pmatrix} = \overline{\mathbf{U}}_3(\mathbf{E}_\mathrm{i})\langle\mathbf{D}\rangle = \overline{\mathbf{U}}_3(\mathbf{E}_\mathrm{i})\overline{\mathbf{U}}_1(\theta,\varphi,kr)\langle\mathbf{S}\rangle \tag{F1}$$

As Equation (F1) evidences, one needs to calculate the rotationally-averaged dipolar vector $\langle\mathbf{D}\rangle = \overline{\mathbf{U}}_1(\theta,\varphi,kr)\langle\mathbf{S}\rangle$, where

$$\langle\mathbf{D}\rangle = \frac{1}{2\pi}\int_0^{2\pi} \mathbf{D}(\alpha_1,\alpha_2,\mathbf{E}_\mathrm{i},\beta)\, d\beta \tag{F2}$$

To obtain a closed-analytical relation of $\langle\mathbf{D}\rangle$, the following identities are needed:

$$\frac{1}{2\pi}\int_0^{2\pi}\cos^4\beta d\beta = \frac{1}{2\pi}\int_0^{2\pi}\sin^4\beta d\beta = \frac{3}{8}, \qquad \frac{1}{2\pi}\int_0^{2\pi}\sin^2\beta\cos^2\beta d\beta = \frac{1}{8}, \qquad \frac{1}{2\pi}\int_0^{2\pi}\cos^2 2\beta d\beta = \frac{1}{2} \tag{F3}$$

Expanding Equation (F2) using the previous identities, it is not difficult to arrive at

$$\frac{\langle|p_x|^2\rangle}{(\epsilon_h\epsilon_0)^2} = \frac{1}{8}\left[\left(3|E_x|^2+|E_y|^2\right)\left(|\alpha_1|^2+|\alpha_2|^2\right) + 2\Re\{\alpha_1\alpha_2^*\}\left(|E_x|^2-|E_y|^2\right)\right] \tag{F4}$$

$$\frac{\langle|p_y|^2\rangle}{(\epsilon_h\epsilon_0)^2} = \frac{1}{8}\left[\left(3|E_y|^2+|E_x|^2\right)\left(|\alpha_1|^2+|\alpha_2|^2\right) - 2\Re\{\alpha_1\alpha_2^*\}\left(|E_x|^2-|E_y|^2\right)\right] \tag{F5}$$

$$\frac{\langle\Re\{p_x p_y^*\}\rangle}{(\epsilon_h\epsilon_0)^2} = \frac{1}{4}\Re\{E_x E_y^*\}\left(|\alpha_1|^2+|\alpha_2|^2+2\Re\{\alpha_1\alpha_2^*\}\right), \qquad \frac{\langle\Im\{p_x p_y^*\}\rangle}{(\epsilon_h\epsilon_0)^2} = \frac{1}{2}\Im\{E_x E_y^*\}\Re\{\alpha_1\alpha_2^*\} \tag{F6}$$

Notable results are now reached: the $\Im\{\alpha_1\alpha_2^*\}$ term vanishes in the averaging process. This result is independent of the incident electromagnetic field $\mathbf{E}_\mathrm{i}$. The previous relations can be written in matrix representation as:

$$\begin{pmatrix} \langle|p_x|^2\rangle \\ \langle|p_y|^2\rangle \\ \langle\Re\{p_x p_y^*\}\rangle \end{pmatrix} = \frac{(\epsilon_h\epsilon_0)^2}{8}\begin{pmatrix} (3|E_x|^2+|E_y|^2) & (3|E_x|^2+|E_y|^2) & 2(|E_x|^2-|E_y|^2) \\ (|E_x|^2+3|E_y|^2) & (|E_x|^2+3|E_y|^2) & 2(|E_y|^2-|E_x|^2) \\ 2\Re\{E_x E_y^*\} & 2\Re\{E_x E_y^*\} & 4\Re\{E_x E_y^*\} \end{pmatrix}\begin{pmatrix} |\alpha_1|^2 \\ |\alpha_2|^2 \\ \Re\{\alpha_1\alpha_2^*\} \end{pmatrix} \tag{F7}$$

By inspecting Equation (F7), one can notice that the matrix is singular since its first and second columns are identical. Therefore, a general 4x4 $\overline{\mathbf{U}}_3(\mathbf{E}_\mathrm{i})$ matrix cannot be found. However, one can still can manipulate Equation (F7) to link $\langle\mathbf{D}\rangle$ with the polarizabilities α_1 and α_2. I now show two simple examples. First, I consider a CP field satisfying $\mathbf{E}_\mathrm{i} = E_0(1,\mathrm{i})/\sqrt{2}$. In this setting, I can write

$$\begin{pmatrix} \langle|p_x|^2\rangle \\ \langle\Im\{p_x p_y^*\}\rangle \end{pmatrix} = \frac{|E_0\epsilon_h\epsilon_0|^2}{4}\begin{pmatrix} 1 & 0 \\ 0 & -1 \end{pmatrix}\begin{pmatrix} |\alpha_1|^2+|\alpha_2|^2 \\ \Re\{\alpha_1\alpha_2^*\} \end{pmatrix} \tag{F8}$$

By inverting this relation, I arrive at

$$\begin{pmatrix} \tilde{\mathcal{P}}_0 \\ \tilde{\mathcal{P}}_1 \end{pmatrix} = \begin{pmatrix} |\alpha_1|^2+|\alpha_2|^2 \\ \Re\{\alpha_1\alpha_2^*\} \end{pmatrix} = \frac{4}{|E_0\epsilon_h\epsilon_0|^2}\begin{pmatrix} 1 & 0 \\ 0 & -1 \end{pmatrix}\begin{pmatrix} \langle|p_x|^2\rangle \\ \langle\Im\{p_x p_y^*\}\rangle \end{pmatrix} \tag{F9}$$

At this point, one needs to reshape the previous relation to find the 4x4 $\overline{\mathbf{U}}_3(\mathbf{E}_\mathrm{i})$ matrix for $\mathbf{E}_\mathrm{i} = E_0(1,\mathrm{i})/\sqrt{2}$. That is,

$$\begin{pmatrix} \tilde{\mathcal{P}}_0 \\ \tilde{\mathcal{P}}_1 \\ 0 \\ 0 \end{pmatrix} = \begin{pmatrix} \left(|\alpha_1|^2+|\alpha_2|^2\right) \\ \Re\{\alpha_1\alpha_2^*\} \\ 0 \\ 0 \end{pmatrix} = \frac{4}{|E_0\epsilon_h\epsilon_0|^2}\begin{pmatrix} 1 & 0 & 0 & 0 \\ 0 & 0 & 0 & 0 \\ 0 & 0 & 0 & 0 \\ 0 & 0 & 0 & -1 \end{pmatrix}\begin{pmatrix} \langle|p_x|^2\rangle \\ \langle|p_y|^2\rangle \\ \langle\Re\{p_x p_y^*\}\rangle \\ \langle\Im\{p_x p_y^*\}\rangle \end{pmatrix} \tag{F10}$$

By inspecting this relation, one can realize that

$$\overline{\mathbf{U}}_3(\mathbf{E}_\mathrm{i} = E_0(1,\mathrm{i})/\sqrt{2}) = \frac{4}{|E_0\epsilon_h\epsilon_0|^2)}\begin{pmatrix} 1 & 0 & 0 & 0 \\ 0 & 0 & 0 & 0 \\ 0 & 0 & 0 & 0 \\ 0 & 0 & 0 & -1 \end{pmatrix} \tag{F11}$$

Next, I consider a LP field satisfying $\mathbf{E}_\mathrm{i} = E_0(0,1)$. In this setting, I can write

$$\begin{pmatrix} \langle|p_x|^2\rangle \\ \langle|p_y|^2\rangle \end{pmatrix} = \frac{|E_0\epsilon_h\epsilon_0|^2}{8}\begin{pmatrix} 1 & -2 \\ 3 & 2 \end{pmatrix}\begin{pmatrix} |\alpha_1|^2+|\alpha_2|^2 \\ \Re\{\alpha_1\alpha_2^*\} \end{pmatrix} \tag{F12}$$

Inverting this equation yields

$$\begin{pmatrix}\tilde{\mathcal{P}}_0\\ \tilde{\mathcal{P}}_1\end{pmatrix}=\begin{pmatrix}|\alpha_1|^2+|\alpha_2|^2\\ \Re\{\alpha_1\alpha_2^*\}\end{pmatrix}=\frac{1}{|E_0\epsilon_h\epsilon_0|^2}\begin{pmatrix}2 & 2\\ -3 & 1\end{pmatrix}\begin{pmatrix}\langle|p_x|^2\rangle\\ \langle|p_y|^2\rangle\end{pmatrix} \tag{F13}$$

At this point, one needs to reshape the previous expression to find the 4x4 $\overline{\mathbf{U}}_3(\mathbf{E}_\mathrm{i})$ matrix for $\mathbf{E}_\mathrm{i}=E_0(0,1)$. That is,

$$\begin{pmatrix}\tilde{\mathcal{P}}_0\\ \tilde{\mathcal{P}}_1\\ 0\\ 0\end{pmatrix}=\begin{pmatrix}\left(|\alpha_1|^2+|\alpha_2|^2\right)\\ \Re\{\alpha_1\alpha_2^*\}\\ 0\\ 0\end{pmatrix}=\frac{1}{|E_0\epsilon_h\epsilon_0|^2}\begin{pmatrix}2 & 2 & 0 & 0\\ -3 & 1 & 0 & 0\\ 0 & 0 & 0 & 0\\ 0 & 0 & 0 & 0\end{pmatrix}\begin{pmatrix}\langle|p_x|^2\rangle\\ \langle|p_y|^2\rangle\\ \langle\Re\{p_xp_y^*\}\rangle\\ \langle\Im\{p_xp_y^*\}\rangle\end{pmatrix} \tag{F14}$$

By inspecting this relation, one can note that

$$\overline{\mathbf{U}}_3(\mathbf{E}_\mathrm{i}=E_0(0,1))=\frac{1}{|E_0\epsilon_h\epsilon_0|^2}\begin{pmatrix}2 & 2 & 0 & 0\\ -3 & 1 & 0 & 0\\ 0 & 0 & 0 & 0\\ 0 & 0 & 0 & 0\end{pmatrix} \tag{F15}$$